2019 IEEE Intelligent Transportation Systems Conference (ITSC)
Auckland, NZ, October 27-30, 2019

# Maneuver Identification for Interaction-Aware Highway Lane Change Behavior Planning based on Polygon Clipping and Convex Optimization

Manuel Schmidt[1], Christian Wissing[2], Jan Braun[1], Till Nattermann[2] and Torsten Bertram[1]

***Abstract*— This contribution presents A-D-PolyC$^{\mathrm{QP}}$ (Automated Driving using Polygon Clipping and Quadratic Programming), a framework for lane change behavior planning of automated vehicles on highways. It solves the tactical decision problem that arises through the presence of more than one lane change maneuver variant in traffic scenes. A-D-PolyC$^{\mathrm{QP}}$ derives all variants deterministically using polygon clipping in spatiotemporal domain and is able to deal with lane changes of surrounding traffic participants. All variants are encoded in a directed graph. The nodes in the graph correspond to spatiotemporal free space polygons and allow the derivation of constraints for trajectory optimization in a Frenet-Serret coordinate frame. Novel, linear time-variant Time-To-Collision and Time Gap constraints based on geometric boundaries are introduced. Interaction-awareness is incorporated by forward simulation of the optimized trajectories. Finally each maneuver is assessed and features are calculated that allow the decision for one lane change maneuver by a higher-level function.**

## I. Introduction

This contribution provides a solution for lane change behavior planning of automated vehicles. Behavior planning is architecturally between the mission planning and local trajectory planning layer of automated driving systems. It is triggered by a lane change request, that might arise through dissatisfaction with the current driving lane or requests in order to follow a planned route. Various lane change execution variants arise naturally in complex traffic scenes. The biggest challenges related to behavior planning therefore consist in deterministically deriving all maneuver variants, efficiently representing and finally assessing them. A reliable assessment of each maneuver in turn requires optimized trajectories that are safe and comfortable. This information finally allows a deliberate decision for one lane change maneuver. A-D-PolyC$^{\mathrm{QP}}$ solves all of these challenges.

Fig. 1 shows the functionality that is proposed in this paper. The first stage is denoted as maneuver identification and its input is the static and dynamic environment model. It is initially described in ego-vehicle coordinates $(X, Y)$ refer to Fig. 1 and then transformed to the Frenet-Serret $(L, N)$ coordinate frame using the Lanelet distance transformation [1]. The maneuver identification then derives all possible lane change variants deterministically together with their corresponding optimized trajectories. All variants are encoded in a graph. The second stage is the maneuver assessment.

*This work was supported by ZF Group Düsseldorf, Germany.

[1]M. Schmidt, J. Braun and T. Bertram are with the Institute of Control Theory and Systems Engineering, TU Dortmund University, D-44227 Dortmund, Germany. manuel3.schmidt@tu-dortmund.de

[2]C. Wissing and T. Nattermann are with ZF Group, Active & Passive Safety Technology, D-40547 Düsseldorf, Germany. christian.wissing@zf.com

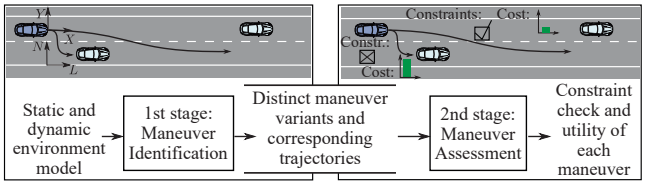


Fig. 1: High-level description of the A-D-PolyC$^{\mathrm{QP}}$ framework.

Each optimized ego trajectory is injected into a forward simulation of the traffic scene to assess the impact of the ego vehicle maneuver onto surrounding traffic participants. The results are passed to a higher-level decision-making and local trajectory planning module.

## II. Related Work and Contribution

The work [2] introduces concepts for the identification of maneuver variants using the notion of homotopy and a Frenet-Serret coordinate frame $(L, N)$. [3] builds upon these foundations and proposes a method to obtain spatiotemporal $(L, t)$ free spaces and optimized lane change trajectories. A similar approach is used in [4]. Here the analysis is conducted in spatial $(L, N)$ domain for discrete times and by aggregation over time, a partitioning of the free space-time is obtained and represented using a graph that has similarities to the one that we propose here. However we obtain the graph using polygon clipping in spatiotemporal $(L, t)$ domain, removing the need to analyze discrete times during graph construction. Reachable set propagation is used in [5] to identify maneuver variants, whereas [6] proposes a directed acyclic graph and $H$-signature calculation to distinguish homotopy classes. Our optimization is mainly inspired by the work of [7] that uses quadratic programming for trajectory optimization. However, lane changes of surrounding traffic are not considered in the aforementioned work. [8] and [9] both propose the use of mixed-integer quadratic programming for trajectory planning. Finally, [10] proposes a sampling framework for behavior planning of automated driving that uses simulations of lower level vehicle controllers and the traffic scene to obtain interaction-aware trajectories.

Our previous approach [11] was able to deterministically identify maneuver variants and introduced a graph structure to represent the traffic scene topology. The trajectory optimization was based on efficient sampling of optimal trajectories with respect to vehicle dynamics, exploiting the spatiotemporal geometry of the traffic scene in $(L, t)$ domain. We assumed in [11] that all surrounding obstacle vehicles stick to their lane. A-D-PolyC$^{\mathrm{QP}}$ generalizes the maneuver identification and removes this assumption such that arbitrary highway scenarios can be handled. The trajectory optimization

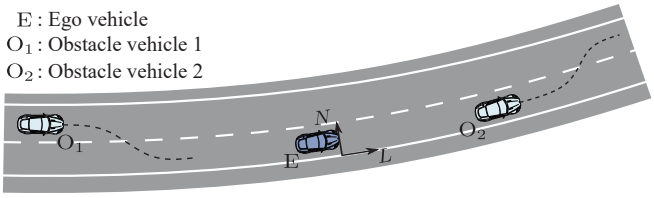


Fig. 2: Exemplary traffic scene with two lane changing obstacle vehicles.

is formulated using convex quadratic programming and can be solved efficiently in real-time. Novel, linear time-variant Time-To-Collision (TTC) and Time Gap (TG) constraints are moreover introduced.

There are four contributions of the paper at hand. The first and main contribution is a functionality to handle lane changes of surrounding obstacle vehicles using polygon clipping in spatiotemporal $(L, t)$ domain and construct a maneuver graph that is able to encode the topology of such complex traffic scenes. Secondly, we present a procedure to identify maneuver variants and to obtain optimization boundaries that are used for separate longitudinal and lateral trajectory planning using convex quadratic programming in the Frenet-Serret frame. Our third contribution enhances safety by integration of linear time-variant TTC and TG constraints into the trajectory optimization. Dense, low-speed traffic scenes can be handled this way in comparison to approaches that use minimum distance constraints only. Finally, we interface the resulting optimized solutions with our approach to interaction awareness presented in [11].

## III. Traffic Scene Topology Analysis

In the maneuver identification stage, refer to Fig. 1, the goal is to identify all possible lane change maneuvers of the ego vehicle. This starts with the systematic analysis of the spatiotemporal traffic scene topology.

### *A. Lane-Discrete Spatiotemporal Free Space Description with Consideration of Obstacle Vehicle Lane Changes*

Consider the synthetic traffic scene in Fig. 2 with the dark blue ego vehicle E and the two light blue obstacle vehicles $\mathrm{O}_1$ and $\mathrm{O}_2$. The dashed, black lines depict the lane change maneuvers of both obstacle vehicles. A-D-Poly$\mathrm{C}^{\mathrm{QP}}$ uses the trajectory prediction module described in [12]. The obtained information also includes a lane association of each obstacle to driving lanes perceived by the ego vehicles sensor system. A driving lane occupancy of an obstacle vehicle $\mathrm{O}_i$ is represented using a spatiotemporal polygon consisting of $n_{\mathrm{O}_i}$ points:

$$P_{\mathrm{O}_i} = \left\{ (L_{\mathrm{O}_i,k}, t_{\mathrm{O}_i,k})_{k=0}^{n_{\mathrm{O}_i}} \right\}. \tag{1}$$

The polygon accounts for the spatial extent of the obstacle vehicles and allows the consideration of safety distances and measurement uncertainties. Based on the predicted, associated lane of each obstacle vehicle, the spatiotemporal free space on each lane is obtained using the difference operation $(\setminus)$ realized with polygon clipping, see [11] for more details. Let $T_{\mathrm{O,LC}}$ be the time instant when an obstacle is assigned for the first time to the target lane of its lane change. We define a fixed transition period $T_{\mathrm{O,LCT}} = 1.3\,\mathrm{s}$ empirically in order to mark the start lane (subscript $(\cdot)_{\mathrm{SL}}$) of the lane change as occupied for the time interval $[0\,\mathrm{s}, T_{\mathrm{O,LC}} + T_{\mathrm{O,LCT}}]$ and the target lane (subscript $(\cdot)_{\mathrm{TL}}$) for $[T_{\mathrm{O,LC}} - T_{\mathrm{O,LCT}}, T_{\max}]$ with the maximum planning time horizon $T_{\max} = 10\,\mathrm{s}$. A-D-Poly$\mathrm{C}^{\mathrm{QP}}$ frequently uses axis-parallel rectangles ranging over the whole longitudinal planning horizon and starting at the times $T_{\mathrm{a}}$ and ending at $T_{\mathrm{b}}$ abbreviated as $P_{\mathrm{rect}}(T_{\mathrm{a}}, T_{\mathrm{b}}) \coloneqq \{(L_{\min}, T_{\mathrm{a}}), (L_{\min}, T_{\mathrm{b}}), (L_{\max}, T_{\mathrm{b}}), (L_{\max}, T_{\mathrm{a}})\}$. Using the difference operation $(\setminus)$ on the start lane of the ego vehicle and considering all obstacle occupancies, one obtains the spatiotemporal free space as a set of distinct polygons $P_i$:

$$\{P_i\} = P_{\mathrm{SL}} \setminus \{P_{\mathrm{O}_i}\}, \tag{2}$$

with the rectangular polygon $P_{\mathrm{SL}} = P_{\mathrm{rect}}(0\,\mathrm{s}, T_{\max})$ that represents the spatiotemporal free space on the start lane for the case of complete absence of obstacle vehicles on that lane. Herein $L_{\min}$ and $L_{\max}$ denote the minimum and maximum longitudinal planning horizon. The same procedure is applied to obtain the set of spatiotemporal free space areas on the target lane. Let $T_{\mathrm{C},k}$ denote time instants when a lane occupancy begins or ends. There are two such time instants in our example on the starting lane of the ego vehicle, refer to the leftmost part of Fig. 3, $T_{\mathrm{C},1} = 2.1\,\mathrm{s}$ and $T_{\mathrm{C},2} = 4\,\mathrm{s}$. The following three polygons are formed in the example case: $P_{\mathrm{SL,O1}} = P_{\mathrm{rect}}(0\,\mathrm{s}, T_{\mathrm{C},1})$, $P_{\mathrm{SL,O2}} = P_{\mathrm{rect}}(T_{\mathrm{C},1}, T_{\mathrm{C},2})$ and $P_{\mathrm{SL,O3}} = P_{\mathrm{rect}}(T_{\mathrm{C},2}, T_{\max})$. Using polygon clipping with the intersection operation $(\cap)$ of both sets of polygons $\{P_i\}$ and $\{P_{\mathrm{SL,Oj}}\}$ one obtains in the exemplary traffic scene a total of seven spatiotemporal free space areas, refer to the leftmost part of Fig. 3.

The notation $\textcircled{\cdot}$ represents the respective polygon $P_{(\cdot)}$. In the example case the areas ④ and ⑥ as well as ⑤ and ⑦ can be combined using a union operation $(\cup)$ on the respective polygons. This reduction of the number of distinct areas reduces complexity. The criterion for joining two polygons is that they have a joint edge at a temporal division line. Next, the adjacency of all nodes of the start lane are checked for connectivity with the start node ① of the ego vehicle. Unreachable nodes, as for example the resulting fused node of ④ and ⑥, are removed. Finally only four distinct spatiotemporal areas remain on the start lane of the ego vehicle as shown in second graph from the left in Fig. 3. Using the same procedure on the target lane, five areas arise as shown in the rightmost part of Fig. 3. The intersection operation of all areas of the start lane with the areas of the target lane and application of the aforementioned fusion mechanism results in three distinct lane change areas ⑤, ⑥ and ⑦ in Fig. 3. They describe spatiotemporal free space simultaneously on both the start and target lane and represent areas in which lateral movement of the ego vehicle is permitted.

### *B. Complete Traffic Scene Topology Graph*

Using the procedure described in the previous section III-A, A-D-Poly$\mathrm{C}^{\mathrm{QP}}$ keeps track of all polygon clipping operations and maintains adjacency relations between all spatiotemporal areas. Fig. 4 shows the resulting graph that encodes the traffic

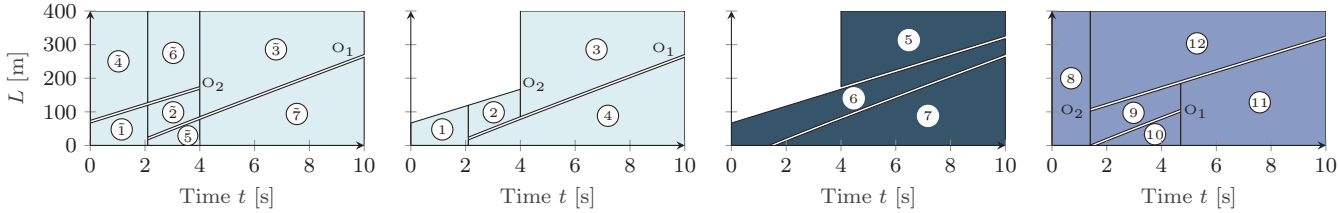


Fig. 3: Spatiotemporal free space areas for the traffic scene shown in Fig. 2 with surrounding obstacle vehicle lane changes. From left to right, the plots depict: The detailed polygons of the start lane of the ego vehicle; unified polygons of the start lane of the ego vehicle; lane change area polygons; unified target lane area polygons.

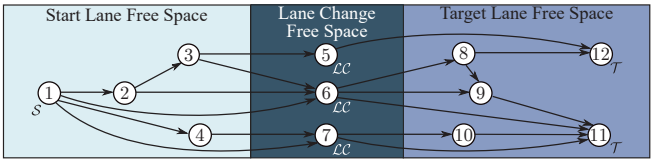


Fig. 4: Graph encoding the traffic scene topology corresponding to the spatiotemporal free space areas and adjacencies shown in Fig. 3.

scene topology. Specific paths in this graph represent lane change execution variants of the ego vehicle. The ego vehicle starts at $(L_{\mathrm{E},0}, t_{\mathrm{E},0}) = (0\,\mathrm{m}, 0\,\mathrm{s})$ so that area ① represents the start node in the graph and is marked with the symbol $\mathcal{S}$. The nodes that correspond to lane change areas are marked with the symbol $\mathcal{LC}$. All target areas are marked with the symbol $\mathcal{T}$ (⑪ and ⑫). Both areas are characterized by the fact, that their right boundary includes the maximum planning time horizon $T_{\max} = 10\,\mathrm{s}$. Maneuver execution variants correspond to paths starting in node ①, passing through exactly one lane change node (⑤, ⑥ or ⑦) and ending in one of the final nodes, either ⑪ or ⑫.

Three exemplary paths in the graph are depicted in Fig. 5. The leftmost one corresponds to the maneuver ①→⑥→⑪ where the ego vehicle conducts its lane change between both obstacle vehicles. The middle figure represents the maneuver ①→②→③→⑤→⑫. Here the ego vehicle waits for the leading obstacle vehicle $O_2$ to change to the left lane then overtakes it on the right side and finally changes lane in front of it. Analysis of the reachable set shows that this maneuver can be achieved within the maximum planning horizon when driving almost at the acceleration limits. The right figure corresponds to the maneuver ①→⑦→⑪. Here the ego vehicle would brake to fall behind the trailing vehicle $\mathrm{O}_1$ and then execute the lane change to the left lane. Inspection of the reachable set of the ego vehicle reveals that the maneuver is not feasible since the small transition corridor of area ① to the lane change area ⑦ can not be reached with the defined acceleration limits of the ego vehicle. Another important maneuver is represented by the path ①→⑥→⑧→⑫ that corresponds to overtaking the vehicle $O_2$ on the start lane of the ego vehicle before the obstacle vehicle $O_2$ conducts its own lane change.

### C. Maneuver Identification and Derivation of Safety Constraints based on spatiotemporal Boundaries

A-D-Poly$\mathrm{C}^{\mathrm{QP}}$ distinguishes immediate and delayed lane changes. An immediate lane change corresponds to spatiotemporal lane change areas that include the point $(0\,\mathrm{m}, 0\,\mathrm{s})$ such that a lateral movement can be immediately initiated, see for example area ⑥ in Fig. 3. Delayed lane changes are characterized by the fact that the ego vehicle has to first stick to its own lane for a certain amount of time in order to reach a lane change area. Both variants are handled differently. Let us first define some relevant notions. The pre-region is the time interval $[0, T_{\mathrm{pre}}]$ on the start lane. A peri-region represents the time interval $(T_{\mathrm{pre}}, T_{\mathrm{peri}}]$ in which a lateral movement to the target lane is realized. Finally, the post-region is the interval $(T_{\mathrm{peri}}, T_{\max}]$ on the target lane of the respective lane change maneuver. Refer to [7] for a detailed description of these regions. A lane change maneuver is unambiguously defined by a path in the graph and the determination of the start time $T_{\mathrm{pre}}$ and end time $T_{\mathrm{peri}}$ of the lateral movement. A method for obtaining these times is described next.

The polygons of lane change maneuver paths in the graph of Fig. 4 include the information of obstacle vehicle positions and velocities. This allows the formulation of linear time-variant TTC and TG safety constraints. The definition of a TG and TTC in the Frenet-Serret coordinate frame at a query time $T_{\mathrm{q}}$ is as follows:

$$T_{\mathrm{TG}}(T_{\mathrm{q}}) = \frac{L_{\mathrm{L}}(T_{\mathrm{q}}) - L_{\mathrm{F}}(T_{\mathrm{q}})}{\dot{L}_{\mathrm{F}}(T_{\mathrm{q}})}, \tag{3}$$

$$T_{\mathrm{TTC}}(T_{\mathrm{q}}) = \frac{L_{\mathrm{L}}(T_{\mathrm{q}}) - L_{\mathrm{F}}(T_{\mathrm{q}})}{\dot{L}_{\mathrm{F}}(T_{\mathrm{q}}) - \dot{L}_{\mathrm{L}}(T_{\mathrm{q}})}. \tag{4}$$

Herein the subscripts $(\cdot)_{\mathrm{F}}$ and $(\cdot)_{\mathrm{L}}$ denote the current follower and leader vehicle. Both safety constraints play a central role in the section on the trajectory optimization. Now, consider for example the lane change area ⑥ in the graph in Fig. 4 and its spatiotemporal extent in Fig. 3. It is necessary to derive the time durations of the pre-, peri- and post-regions of the lane change maneuver. The times $T_{\mathrm{pre}}$ and $T_{\mathrm{peri}}$ are the two degrees of freedom. They are chosen using a prior safety evaluation of the spatiotemporal lane change area. We identify the time interval $[T_1, T_2]$ by analyzing the time gap equation (3) using the initial ego vehicle velocity $\dot{L}_{\mathrm{E},0}$ and predicted follower velocity $\dot{L}_{\mathrm{F}}(t)$. A minimum spatial gap is defined as: $L_{\mathrm{minGap}}(t) = (\dot{L}_{\mathrm{E},0} + \dot{L}_{\mathrm{F}}(t))T_{\mathrm{TG,min}}$, with the minimum prior Time Gap $T_{\mathrm{TG,min}}$. Next the lower and upper bounds of the lane change area $L_{\mathrm{LC,UB}}(t)$ and $L_{\mathrm{LC,LB}}(t)$ are used to find all intervals that fulfill the constraint: $L_{\mathrm{LC,UB}}(t) - L_{\mathrm{LC,LB}}(t) \geq L_{\mathrm{minGap}}(t)$. The next step is marking intervals as infeasible in case they are shorter than a user-defined minimum lane change time $T_{\mathrm{LC,min}}$. The distinction between immediate and delayed lane changes is taken into account. In case of an immediate lane change, the longest interval is found and

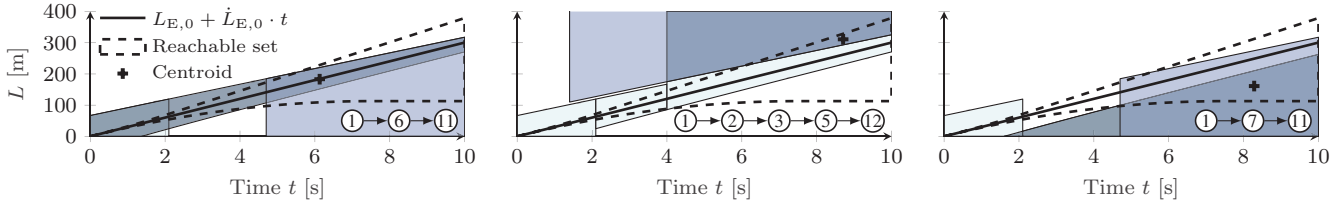


Fig. 5: Three exemplary lane change maneuver paths that the graph in Fig. 4 encodes.

checked if it is longer than the maximum lane change time $T_{\mathrm{LC,max}}$. If that is the case, then the peri-region is then chosen to be $(T_{\mathrm{pre}}, T_{\mathrm{peri}}] = (T_1, T_1 + T_{\mathrm{LC,max}}]$, else $(T_{\mathrm{pre}}, T_{\mathrm{peri}}] = (T_1, T_2]$. Therefore taking into account that immediate lane changes should start as early as possible. In the case of delayed lane changes the same check against the maximum lane change time is done. If the interval is longer, then the peri-region is chosen to be $(T_{\mathrm{pre}}, T_{\mathrm{peri}}] = (T_2 - T_{\mathrm{LC,max}}, T_2]$, else $(T_{\mathrm{pre}}, T_{\mathrm{peri}}] = (T_1, T_2]$. The idea is to conduct a delayed lane change as late as possible to reduce the need for decelerations. The durations of the pre- and post-regions are then obtained as the remaining times prior and after the peri-region in the planning horizon. If A-D-PolyC$^{\mathrm{QP}}$ was applied with a receding horizon, the durations would be adapted according to the lateral progress towards the target lane.

At this point, there is still ambiguity left since a path consists of possibly multiple traversed areas in the start lane, exactly one lane change area and possible multiple traversed target lane areas. Two Dijkstra shortest path searches with unit cost on the edges in the graph are used to obtain the complete maneuver path. For each lane change area, the start lane free space corresponding to $T_{\mathrm{pre}}$ is found and a search from that area in backward direction to area ① is conducted. Another search in forward direction from the target area node corresponding to $T_{\mathrm{peri}}$ to all areas in the set $\mathcal{T}$ completes the path. Only the shortest path is picked for the forward direction search in case that several paths are found. This procedure integrates the preference to traverse as few areas as possible.

## IV. Maneuver Identification, Optimization and Traffic Interaction Assessment

This section introduces the maneuver optimization and assessment of the resulting trajectories. It is based on formulating and solving two convex quadratic programs for the longitudinal and lateral motion. The resulting trajectories are finally injected in a forward simulation to assess the impact on the whole traffic scene.

### *A. Safe Motion Planning using Convex Quadratic Programming and Interaction-Awareness*

The system model used for the motion planning within the contribution at hand is a triple integrator for both the lateral and longitudinal movement of the vehicle. The time discrete description of the system dynamics is obtained using the theory of sampled data systems. We assume that the control input, in our case the longitudinal and lateral jerk, is piecewise constant during each sampling interval. Assume that for each lane change maneuver $i$ there exist lower and upper bounds for the longitudinal and lateral movement, determined by the pre-, peri- and post-region of the maneuver. These are $L_{i,\mathrm{UB}}(k)$, $L_{i,\mathrm{LB}}(k)$, $N_{i,\mathrm{UB}}(k)$ and $N_{i,\mathrm{LB}}(k)$. The trajectory optimization problem is formulated similarly to [7]. It is however conducted in the Frenet-Serret coordinate frame to deal with curvy highway scenarios using the following small angle approximations $\ddot{L} \approx \ddot{X}$ and $\ddot{N} \approx \ddot{Y} - \kappa(L)\dot{L}^2$, with the curvature of the reference lane at the coordinate $L$ of the Frenet-Serret frame $\kappa(L)$. The longitudinal cost function is defined as:

$$J_L = \sum_{k=1}^{N_p} \left( \alpha_0 \left( \dot{L}_{\mathrm{E}}(k) - \dot{L}_{\mathrm{d}}(k) \right)^2 + \alpha_1 \ddot{L}_{\mathrm{E}}(k)^2 + \alpha_2 L_{\mathrm{E}}^{(3)}(k)^2 \right), \tag{5}$$

with the desired longitudinal velocity $\dot{L}_{\mathrm{d}}(k)$, weighting factors $\alpha_j \in \mathbb{R}_{++}, j \in \{0,1,2\}$ and the last sample $N_{\mathrm{p}} \in \mathbb{N}$. The longitudinal optimization is subject to the constraints:

$$\begin{aligned} L_{\mathrm{LB}}(k) \leq L_{\mathrm{E}}(k) \leq L_{\mathrm{UB}}(k), \\ \dot{L}_{\min} \leq \dot{L}_{\mathrm{E}}(k) \leq \dot{L}_{\max}, \\ \ddot{X}_{\min} \leq \ddot{L}_{\mathrm{E}}(k) \leq \ddot{X}_{\max}, \\ L_{\min}^{(3)} \leq L_{\mathrm{E}}^{(3)} \leq L_{\max}^{(3)}, \end{aligned} \tag{6}$$

$$\begin{aligned} L_{\mathrm{E}}(k+1) &= L_{\mathrm{E}}(k) + \dot{L}_{\mathrm{E}}(k)h + \ddot{L}_{\mathrm{E}}(k)\frac{h^2}{2} + L_{\mathrm{E}}^{(3)}(k)\frac{h^3}{6}, \\ \dot{L}_{\mathrm{E}}(k+1) &= \dot{L}_{\mathrm{E}}(k) + \ddot{L}_{\mathrm{E}}(k)h + L_{\mathrm{E}}^{(3)}(k)\frac{h^2}{2}, \\ \ddot{L}_{\mathrm{E}}(k+1) &= \ddot{L}_{\mathrm{E}}(k) + L_{\mathrm{E}}^{(3)}(k)h, \\ L_{\mathrm{E}}(0) &= L_{\mathrm{E},0}, \quad \dot{L}_{\mathrm{E}}(0) = \dot{L}_{\mathrm{E},0}, \quad \ddot{L}_{\mathrm{E}}(0) = \ddot{L}_{\mathrm{E},0}, \end{aligned} \tag{7}$$

with the stepsize $h \in \mathbb{R}_{++}$. The jerk $L_{\mathrm{E}}^{(3)}(k)$ acts as the control input. Further constraints are added to account for minimum TTC and TG. Using the upper and lower boundaries $L_{i,\mathrm{UB}}(k)$ and $L_{i,\mathrm{LB}}(k)$, the constraints are:

$$\begin{aligned} L_{\mathrm{LB}}(k + N_{\mathrm{TTC}}) \leq L_{\mathrm{E}}(k) + \dot{L}_{\mathrm{E}}(k) T_{\mathrm{TTC,min}} \\ L_{\mathrm{E}}(k) + \dot{L}_{\mathrm{E}}(k) T_{\mathrm{TTC,min}} \leq L_{\mathrm{UB}}(k + N_{\mathrm{TTC}}), \\ T_{\mathrm{TG,min}} \dot{L}_{\mathrm{E}}(k) + L_{\mathrm{E}}(k) \leq L_{\mathrm{UB}}(k), \\ L_{\mathrm{LB}}(k + N_{TG}) \leq L_{\mathrm{E}}(k), \end{aligned} \tag{8}$$

with the number of samples $N_{\mathrm{TG}} = \lceil \frac{T_{\mathrm{TG,min}}}{h} \rceil \in \mathbb{N}$ and $N_{\mathrm{TTC}} = \lceil \frac{T_{\mathrm{TTC,min}}}{h} \rceil \in \mathbb{N}$ corresponding to the minimum TTC and TG times. The TTC and TG constraints are derived from their geometric meaning in spatiotemporal $(L,t)$ domain. This formulation results in a convex quadratic program that is solved using the OSQP solver [13]. The lateral trajectory optimization is conducted after obtaining

the optimal longitudinal trajectory $L_{\mathrm{E}}^*(k)$. The following cost function is optimized:

$$J_N = \sum_{k=1}^{N_p} \Big( \beta_0 \left( N_{\mathrm{E}}(k) - N_{\mathrm{d}}(k) \right)^2 + \beta_1 \dot{N}_{\mathrm{E}}(k)^2 + \\ + \beta_2 \ddot{N}_{\mathrm{E}}(k)^2 + \beta_3 N_{\mathrm{E}}^{(3)}(k)^2 \Big), \tag{9}$$

with weighting factors $\beta_j \in \mathbb{R}_{++}, j \in \{0,1,2,3\}$. $N_{\mathrm{d}}(k)$ represents a lateral tracking reference. It helps to push the trajectory further away from the upper and lower boundaries $N_{\mathrm{LB}}(k)$ and $N_{\mathrm{UB}}(k)$ and is further examined in section V. The lateral optimization is subject to the analogous system dynamics and initial value constraints as in equation (7). Furthermore, the following set of constraints is applied:

$$\begin{aligned} N_{\mathrm{LB}}(k) \leq N_{\mathrm{E}}(k) \leq N_{\mathrm{UB}}(k), \\ \dot{L}_{\mathrm{E}}^*(k)\tan(-\theta_{\max}) \leq \dot{N}_{\mathrm{E}}(k) \leq \dot{L}_{\mathrm{E}}^*(k)\tan(\theta_{\max}), \\ \ddot{Y}_{\min} - \kappa(L_{\mathrm{E}}^*(k))(\dot{L}_{\mathrm{E}}^*(k))^2 \leq \ddot{N}_{\mathrm{E}}(k), \\ \ddot{Y}_{\max} - \kappa(L_{\mathrm{E}}^*(k))(\dot{L}_{\mathrm{E}}^*(k))^2 \geq \ddot{N}_{\mathrm{E}}(k), \end{aligned} \tag{10}$$

The trajectory optimization problem is solved sequentially, starting with the longitudinal optimization and finally solving the lateral problem. This allows to consider the coupling between $L_{\mathrm{E}}$ and $N_{\mathrm{E}}$ and to account for a maximum heading angle $\theta_{\max} \in \mathbb{R}_{++}$. A-D-PolyC$^{\mathrm{QP}}$ plans comfortable lane change maneuvers with tight and conservative bounds using simplified motion models in form of two triple integrator systems. This choice is justified since A-D-PolyC$^{\mathrm{QP}}$ is used prior to a local trajectory planner in an automated driving system that has less conservative bounds and uses high fidelity vehicle models to cater for nonlinear effects.

## V. Evaluation

This section presents results of the application of A-D-PolyC$^{\mathrm{QP}}$ in simulation with focus on the maneuver optimization. The nomenclature used is shown in Fig. 6. We choose a highway entry scenario with a total of four obstacle vehicles. The simulation environment described in [14] is used. A-D-PolyC$^{\mathrm{QP}}$ is triggered by a lane change request to the left and identifies maneuver variants for every time step of the simulation. The initial traffic scene configurations are represented in Table I. Each row in Fig. 7 corresponds to a certain time step of the simulation and shows results of A-D-PolyC$^{\mathrm{QP}}$. They are all obtained using the following set of parameters: $\{\alpha_0 = 1,\ \alpha_1 = 2,\ \alpha_2 = 2.5, \beta_0 = 2,\ \beta_1 = 2,\ \beta_2 = 2.5,$ $\beta_3 = 5,\ h = 0.5\,\mathrm{s},\ T_{\mathrm{TTC,min}} = 5\,\mathrm{s},\ T_{\mathrm{TG,min}} = 1\,\mathrm{s}\}$. The optimized trajectories are then injected into the forward simulation of the traffic scene using [12] for an assessment of the traffic interaction based on generalized kinetic energies as introduced in [11]. Finally, ego vehicle dynamics and situation features for all three time steps are shown in Table II. The desired longitudinal velocity is set to $\dot{L}_{\mathrm{d}}(k) = 38.9\,\frac{\mathrm{m}}{\mathrm{s}}$. The graphs corresponding to each situation encodes at least two lane change variants and each row in Fig. 7 always shows the feasible, least total cost $J = J_L + J_N$ solution. The first row shows an immediate lane change maneuver. The ego vehicle has to accelerate since the trailing vehicle $\mathrm{O}_5$ on the target lane is significantly faster than the ego vehicle. Here, the ego vehicle comes close to its desired velocity (refer to Table II). The second row in Fig. 7 shows a configuration in which the ego vehicle has to break significantly in order to execute the lane change within the planning horizon. Note that the simulation environment models fluctuations of traffic participants within their respective lanes and here the ego vehicle is initially not centered within the start lane. Our framework copes with this deviation. Finally the third row of Fig. 7 shows a time step 5 s later than the one in the second row. This time, the ego vehicle does not have to break severely and is able to conduct a more comfortable lane change compared to both other results. The introduction of linear time variant constraints on the TTC and TG results in high values of $T_{\mathrm{TTC}}$ and $T_{\mathrm{TG}}$ in Table II. Therefore, the planned lane changes have desired safety margins. Inspection of the generalized OTP (Obstacle Traffic Participants) energies, refer to [11] for the mathematical definition, also shows that these constraints keep the influence on the obstacle vehicles low. Loosening these constraints results in stronger influences. The values of the generalized kinetic energies of the ego vehicle are proportional to the area between the constant velocity prediction $L_{\mathrm{E},0} + \dot{L}_{\mathrm{E},0}t$ and $L_{\mathrm{E}}^*(t)$, refer to the second column in Fig. 7. This clarifies that the immediate lane change is the least comfortable while keeping with safety margins.

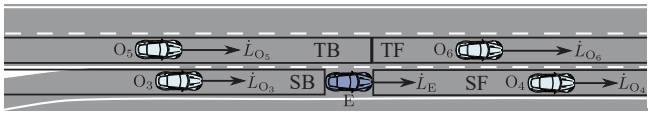


Fig. 6: Nomenclature for the traffic scene description with respect to the ego vehicle as used in section V. SB, SF, TB and TF denote regions behind (B) and in front (F) of the ego vehicle at the start (S) and target (T) lane.

Real-time capability plays a crucial role for the broad application of A-D-PolyC$^{\mathrm{QP}}$. The two major algorithmic parts in our framework consist of the polygon clipping for spatiotemporal traffic scene understanding and the trajectory optimization. The runtime evaluation in Table III reveals that both operations are in the sub-microsecond range and hence fast enough for real-time application of our framework.

## VI. Conclusion and Future Work

This contribution presents A-D-PolyC$^{\mathrm{QP}}$ which solves the lane change behavior planning problem for highway driving. All lane change execution variants based on trajectory predictions of obstacle vehicles are identified systematically for arbitrary highway scenarios using polygon clipping. Our framework deals with lane changes of obstacle vehicles and captures the traffic scene topology using a graph. An efficient procedure for the identification of maneuvers was presented. Safety constraints based on Time-To-Collisions and Time Gaps are incorporated in the trajectory optimization stage using convex quadratic programming. Evaluation in a simulated highway entry scenario shows that smooth and comfortable trajectories are obtained while maintaining safety margins. The runtime analysis shows that real-time constraints are easily met. Our future work aims at tuning parameters and constraints for ride quality.

TABLE I: Initial traffic scene cofigurations corresponding to Fig. 7.

| | $L_{0,(\cdot)}$ | | | | | $\dot{L}_{0,(\cdot)}$ | | | | | $N_{0,(\cdot)}$ | | | | | $\dot{N}_{0,(\cdot)}$ | | | | |
|---|---|---|---|---|---|---|---|---|---|---|---|---|---|---|---|---|---|---|---|---|
| Maneuver in Fig. 7 | E m | $O_3$ m | $O_4$ m | $O_5$ m | $O_6$ m | Ego $\frac{m}{s}$ | $O_3$ $\frac{m}{s}$ | $O_4$ $\frac{m}{s}$ | $O_5$ $\frac{m}{s}$ | $O_6$ $\frac{m}{s}$ | Ego m | $O_3$ m | $O_4$ m | $O_5$ m | $O_6$ m | E $\frac{m}{s}$ | $O_3$ $\frac{m}{s}$ | $O_4$ $\frac{m}{s}$ | $O_5$ $\frac{m}{s}$ | $O_6$ $\frac{m}{s}$ |
| First row | 0 | -38.41 | 53.99 | -81.88 | 101.72 | 17.24 | 14.18 | 17.09 | 26.73 | 23.93 | 1.77 | 1.39 | 2.34 | 5.99 | 6.17 | 0.03 | -0.61 | 0.02 | -0.62 | -0.07 |
| Second row | 0 | -50.64 | 53.97 | -37.53 | / | 19.21 | 16.94 | 19.33 | 27.33 | / | 1.16 | 1.87 | 2.36 | 5.71 | / | -0.05 | -0.06 | -0.05 | -0.18 | / |
| Third row | 0 | -60.95 | 53.98 | -2.36 | / | 19.79 | 17.84 | 20.15 | 24.99 | / | 2.00 | 1.97 | 2.64 | 5.98 | / | 0.14 | 0.06 | -0.03 | -0.02 | / |

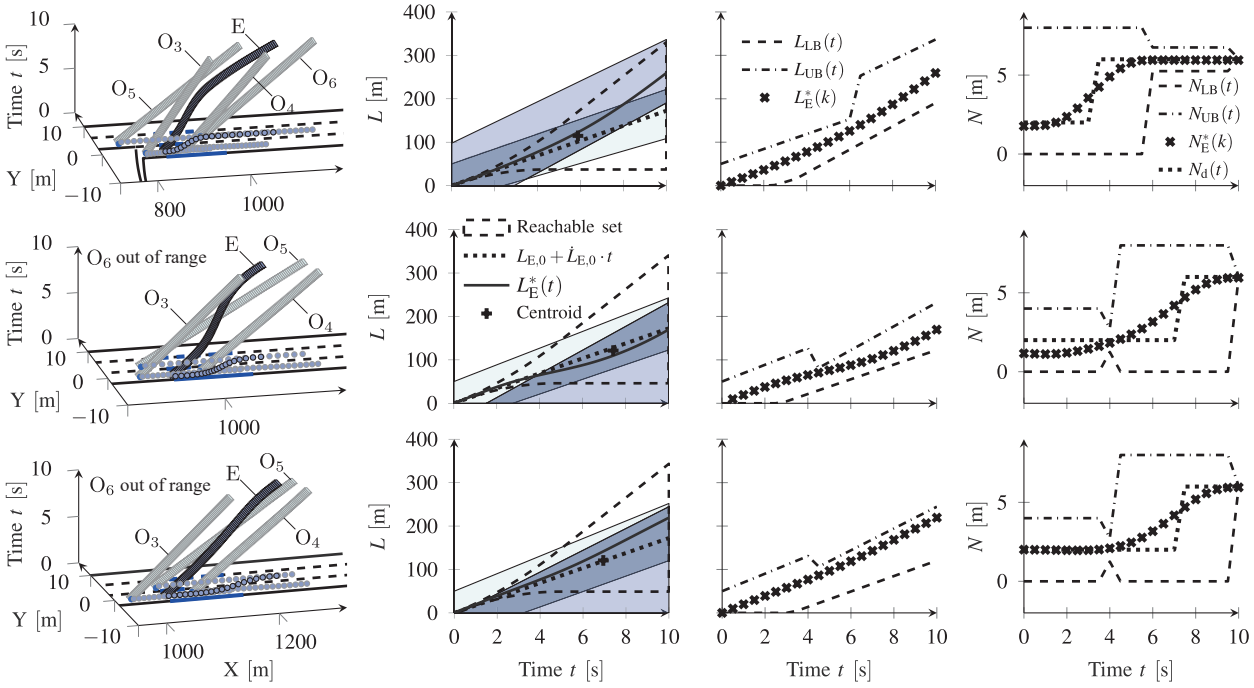


Fig. 7: Results of A-D-PolyC$^{QP}$ for three simulation time steps. The first column shows the traffic scene evolutions in $(L, N, t)$ domain. The second column depicts the spatiotemporal areas and optimized longitudinal trajetories. All sample points of the optimized longitudinal trajectories and boundaries are shown in the third column. The fourth column shows the same quantities for the lateral movement. A stepsize $h = 0.5\,\mathrm{s}$ is used in all optimizations.

TABLE II: Ego vehicle dynamics and situation features corresponding to the optimized ego vehicle trajectories in Fig. 7.

| | $\Delta\dot{L}$ | | $\min(T_{\mathrm{TTC},(\cdot)})$ | | | | $\min(T_{\mathrm{TG},(\cdot)})$ | | | | Energies $E$ | |
|---|---|---|---|---|---|---|---|---|---|---|---|---|
| Maneuver in Fig. 7 | T-0 $\frac{m}{s}$ | T-d $\frac{m}{s}$ | SB s | SF s | TB s | TF s | SB s | SF s | TB s | TF s | OTP J | Ego J |
| First row | 20.8 | -0.8 | $\infty$ | 12.7 | 9.5 | 5.9 | 2.7 | 2.3 | 1.8 | 2.2 | 3.8 | 213.4 |
| Second row | 9.0 | -10.7 | 7.6 | $\infty$ | $\infty$ | 74.0 | 2.1 | 2.8 | $\infty$ | 2.3 | 1.9 | 77.3 |
| Third row | 5.4 | -13.7 | $\infty$ | 9.9 | $\infty$ | 44.2 | 3.4 | 2.0 | 3.4 | 2.0 | 1.1 | 59.3 |

Abbreviations: T-0: Longitudinal velocity difference between ego velocity at beginning and end of lane change, T-d: Long. vel. diff. between ego velocity at end of lane change and desired velocity (here: speed limit on target lane), OTP: Other traffic participants.

TABLE III: Runtime evaluation using 300 simulation steps on a PC with Windows 10 (i5-6500, 16GB RAM). Functions are called as compiled MEX functions from MATLAB.

| | Calls | Total time | Avg. time | Avg. cycle time |
|---|---|---|---|---|
| QP Solver | 645 | 0.344 s | 533 $\mu$s | 1.16 ms |
| Polygon Clipping | 3984 | 0.543 s | 136 $\mu$s | 1.81 ms |

## References


[1] P. Bender, J. Ziegler, and C. Stiller, "Lanelets: Efficient map representation for autonomous driving," in *IEEE Intelligent Vehicles Symposium*, June 2014.

[2] P. Bender, Ö. Ş. Taş, *et al.*, "The combinatorial aspect of motion planning: Maneuver variants in structured environments," in *IEEE Intelligent Vehicles Symposium*, June 2015.

[3] J. Schlechtriemen, K. P. Wabersich, and K. D. Kuhnert, "Wiggling through complex traffic: Planning trajectories constrained by predictions," in *IEEE Intelligent Vehicles Symposium*, June 2016.

[4] F. Altché and A. de La Fortelle, "Partitioning of the free space-time for on-road navigation of autonomous ground vehicles," in *IEEE Conference on Decision and Control*, Dec 2017.

[5] S. Söntges and M. Althoff, "Computing the drivable area of autonomous road vehicles in dynamic road scenes," *IEEE Transactions on Intelligent Transportation Systems*, June 2018.

[6] T. Gu, "Improved trajectory planning for on-road self-driving vehicles via combined graph search, optimization & topology analysis," Ph.D. dissertation, Carnegie Mellon University, 2017.

[7] J. Nilsson, M. Brännström, *et al.*, "Longitudinal and lateral control for automated yielding maneuvers," *IEEE Transactions on Intelligent Transportation Systems*, May 2016.

[8] X. Qian, F. Altché, *et al.*, "Optimal trajectory planning for autonomous driving integrating logical constraints: An miqp perspective," in *IEEE Int. Conf. on Intelligent Transportation Systems*, Nov 2016.

[9] C. Miller, C. Pek, and M. Althoff, "Efficient mixed-integer programming for longitudinal and lateral motion planning of autonomous vehicles," in *IEEE Intelligent Vehicles Symposium*, June 2018.

[10] J. Wei, J. M. Snider, *et al.*, "A behavioral planning framework for autonomous driving," in *IEEE Intelligent Vehicles Symposium*, June 2014.

[11] M. Schmidt, C. Manna, *et al.*, "An interaction-aware lane change behavior planner for automated vehicles on highways based on polygon clipping," *IEEE Robotics and Automation Letters*, April 2019.

[12] C. Wissing, T. Nattermann, *et al.*, "Interaction-aware long-term driving situation prediction," in *IEEE Int. Conf. on Intelligent Transportation Systems*, Nov. 2018.

[13] B. Stellato, G. Banjac, *et al.*, "OSQP: An operator splitting solver for quadratic programs," *ArXiv e-prints*, Nov. 2017.

[14] C. Wissing, T. Nattermann, *et al.*, "Environment simulation for the development, evaluation and verification of underlying algorithms for automated driving," in *Automotive meets Electronics*, March 2016.